Supplementary Information

Growth direction dependent separate-channel charge transport in organic weak charge-transfer co-crystal of anthracene-DTTCNQ

Hui Jiang,* Jun Ye, Peng Hu, Shengli Zhu,* Yanqin Liang, Zhenduo Cui, Christian Kloc, and Wenping Hu*

Abstract: Co-crystallization is an efficient way of molecular crystal engineering to tune the electronic properties of organic semiconductors. In this work, we synthesized anthracene-4,8-bis(dicyanomethylene)4,8-dihydrobenzo[1,2-b:4,5-b']-dithiophene (DTTCNQ) single crystals as a template to study the crystal growth directions dependent on charge transport properties and attempted to elucidate the mechanism by proposing a separate-channel charge transport model. Single-crystal anthracene-DTTCNQ field-effect transistors showed that ambipolar transport properties could be observed in all crystal growth directions. Furthermore, with changing the measured crystal directions, the electronic properties experienced a weak change from n-type dominated ambipolar, balanced ambipolar, to p-type dominated ambipolar properties. The theoretical calculations at density functional theory (DFT) and higher theory levels suggested that the anthracene-DTTCNQ co-crystal motif was a weak charge-transfer complex, in line with the experiment. Furthermore, the detailed theoretical analysis also indicated that electron or hole transport properties originated from separated channels formed by DTTCNQ or anthracene molecules. We thus proposed a novel separate-channel transport mechanism to support additional theoretical analysis and calculations. The joint experimental and theoretical efforts in this work suggest engineering of co-crystallization of weak charge-transfer complexes can be a practical approach in achieving tuneable ambipolar charge transport properties by the rational choice of co-crystal formers.

TABLE OF CONTENTS

1. Results and discussions

1.1 Fig. S1. XRD results of anthracene-DTTCNQ single crystals along the vertical growth direction.

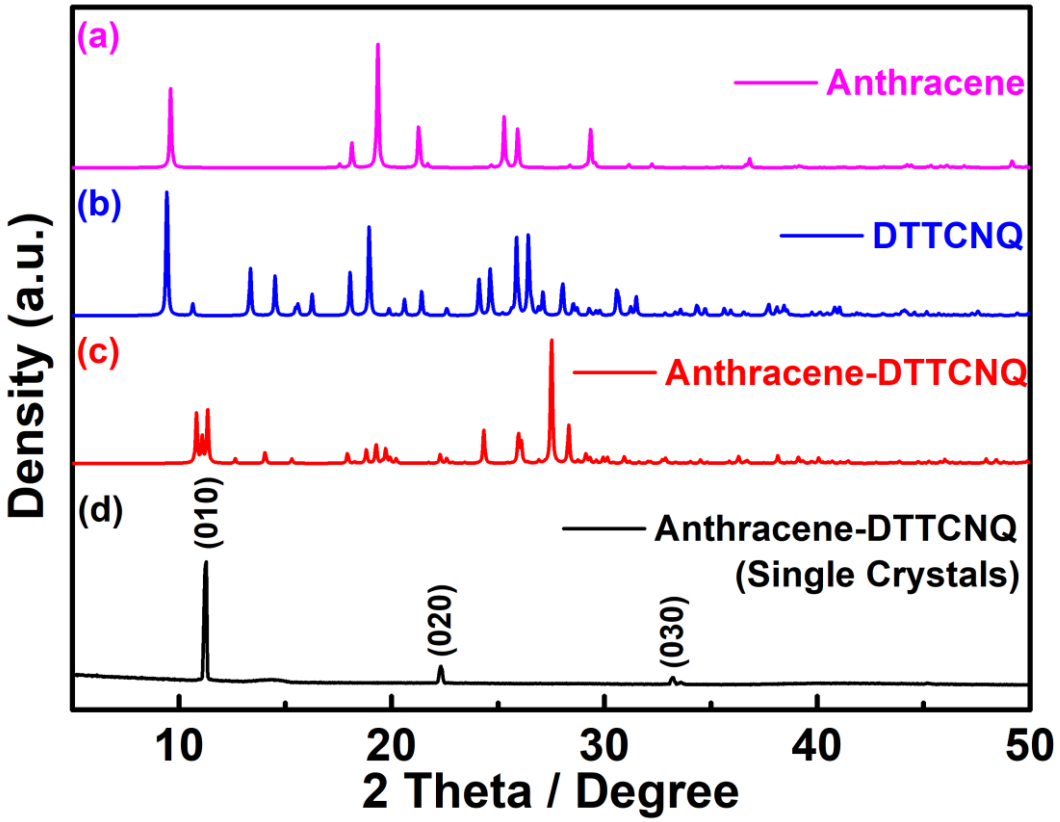

Fig. S1. XRD results of anthracene-DTTCNQ single crystals along the vertical growth direction. (a) XRD results of anthracene. (b) XRD results of DTTCNQ. (c) XRD results of anthracene-DTTCNQ. (d) The measured XRD results of single-crystal anthracene-DTTCNQ solution-dropped on the OTS-modified SiO_2/Si substrate. The source data (single crystal structures) of (a) anthracene and (b) DTTCNQ is downloaded from the Cambridge crystallographic data center (CCDC) database. The XRD data of anthracene-DTTCNQ is generated via our obtained single-crystal structure. (CCDC number: 1915403, anthracene-DTTCNQ)

- **The measured XRD results (Fig. S1d) of single crystal anthracene-DTTCNQ solution-dropped on the OTS-modified SiO_2/Si substrate indicate that the vertical growth direction of single crystal anthracene-DTTCNQ is [010].**

1.2 Fig. S2. IR spectroscopy results of anthracene, DTTCNQ, and anthracene-DTTCNQ.

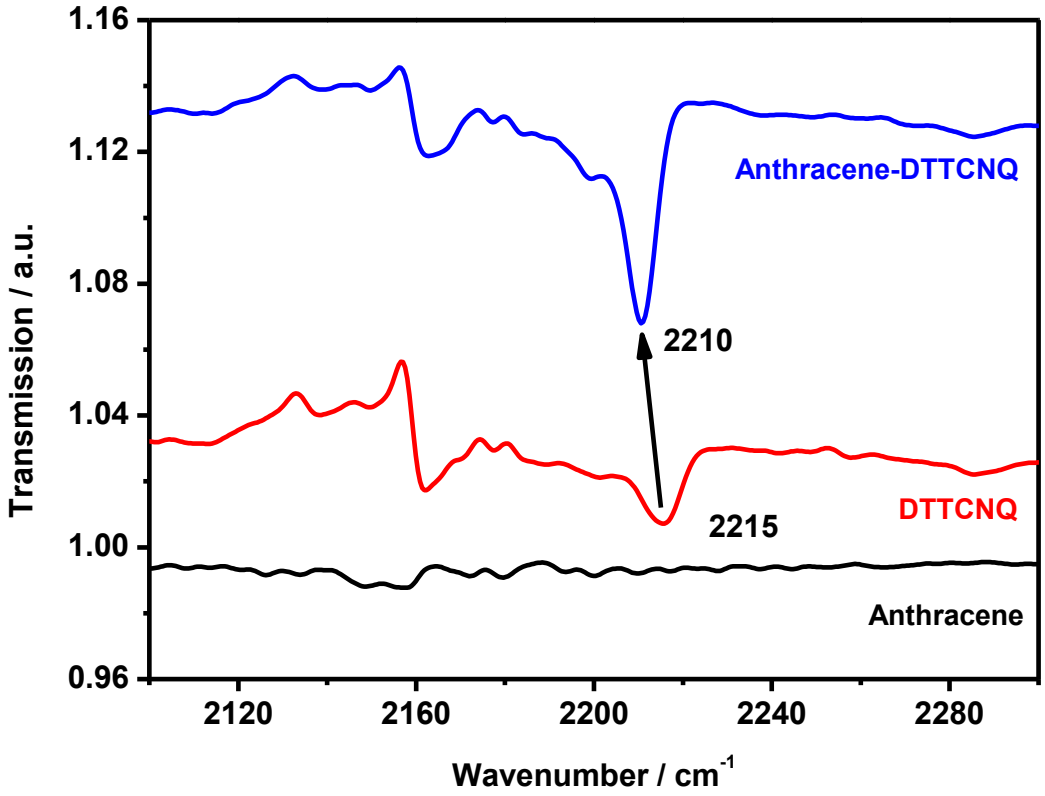

Fig. S2. IR spectroscopy results of anthracene, DTTCNQ, and anthracene-DTTCNQ single crystals.

- **The above Fig. S2 indicates that the C≡N stretching of DTTCNQ is 2215 cm^{-1}. When charge transfer occurs, the C≡N stretching mode is red-shifted compared with pristine DTTCNQ. It agrees with the previous TCNQ-based (such as F_4TCNQ-based, F_6TNAP-based) charge transfer compound (Cryst. Growth Des. 2016, 16, 3019-3027; Cryst. Growth Des. 2018, 18, 1776-1785; J. Mater. Chem. C 2019, 6, 1884-1902). The peak of anthracene-DTTCNQ downshifts 5 cm^{-1}. This value indicates that the degree of charge transfer (DCT) is quite small (in the range of 0.04-0.1). The relation between 5 cm^{-1} peak shift and DCT in different systems is summarized below:**

Charge transfer compounds	DCT	Reference
TCNQ-based	0.08±0.03	*J. Am. Chem. Soc., 1981, 103, 2442-2443*
F_4TCNQ-based	0.06±0.02	*CrystEngComm, 2017, 19, 618-624*
F_6TNAP-based	0.1±0.05	*Cryst. Growth Des. 2018, 18, 1776-1785*

1.3 Fig. S3. The leakage currents of anthracene-DTTCNQ single-crystal field-effect transistors (SCFETs) shown in Fig. 4g-l of the main text.

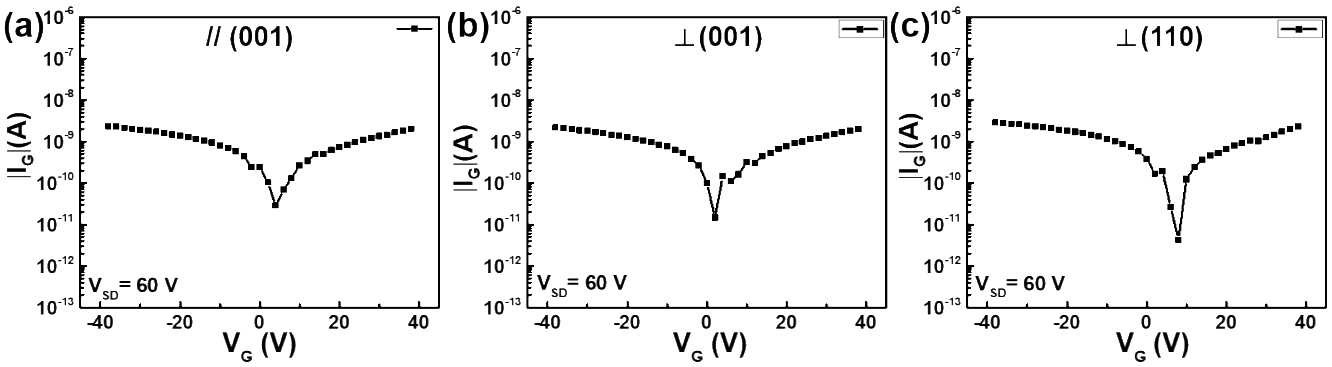

Fig. S3. The leakage currents of anthracene-DTTCNQ single-crystal field-effect transistors (SCFETs) shown in **Fig. 4g-l** of the main text. The device leakage currents (a) along the (001) plane, (b) vertical to the (001) plane, and (c) vertical to the (110) plane shown in **Fig. 4g-l** in the main text.

- **The device leakage current results indicate that the influence of the gate leakage current can be ignored.**

1.4 Brief introduction of the polaron transport theory based on canonical transformation of the generalized Holstein Hamiltonian.

The overall description of the polaron transport theory can be found out in our earlier work.[1, 2] Here we only briefly describe some essential components of the theory. The electron or hole transport is calculated based on a temperature-dependent canonical transformation of Holstein Hamiltonian.[3] The 1D polaron transport model is an extension of the work done by Munn and Silbey[4-6] with variationally determined temperature-dependent canonical transformation parameters. The generalized Holstein Hamiltonian can be written in the following form:

$$H = \sum_n \epsilon a_n^\dagger a_n + \sum_{n,m} t_{nm} a_n^\dagger a_m + \sum_k \omega_k \left(b_k^\dagger b_k + 1/2\right) + N^{-1/2} \sum_{nmk} \omega_k f_{nm}^k a_n^\dagger a_m \left(b_k + b_{-k}^\dagger\right) \quad \text{(S1)}$$

Here $a_n^\dagger(a_n)$ is the creation (annihilation) operator of an electron/hole at site n with energy ϵ, and $b_k^\dagger(b_k)$ creates (destroys) a phonon with the frequency of ω_k and wave vector k. t_{nm} here is the electronic transfer integral between molecules in site n and m. The electron/hole-phonon coupling strength is described by the coupling matrix f_{nm}^k satisfying the relationship of $(f_{n-m}^k)^* = e^{-ik\cdot(R_n - R_m)} f_{n-m}^{-k}$ to make H Hermitian and translational invariant, here R_n is the real space vector of the nth molecule in the crystal. In the original theoretical work,[1, 2] we have taken into consideration both diagonal and off-diagonal elements in f_{nm}^k. In the simplified model, we only considered local molecular vibrational modes k. Thus, thus all off-diagonal elements in f_{nm}^k become zero, leading to simplified relationship between vibrational coupling strength S_k and diagonal elements of the coupling matrix $f_0^k = g_k^n = g_k e^{ik\cdot R_n}$, as $S_k = \frac{1}{2}(g_k)^2$. Also, we take the electronic transfer integrals between nearest-neighbor molecule dimers to simply the calculations.

A key piece of the 1D polaron transport model is the canonical transformation, which can diagonalize the generalized Holstein Hamiltonian in Eq. (S1). The canonical transformation in site space can be written as:

$$H \to \tilde{H} = U^\dagger H U \quad \text{(S2)}$$

with

$$U = exp\left[N^{-1/2} \sum_{nmk} A_{nm}^k \left(b_{-k}^\dagger - b_k\right) a_n^\dagger a_m\right] \quad \text{(S3)}$$

here A_{nm}^k is the transformation matrix to be variationally determined, this will lead to transformed Hamiltonian composing of zeroth-order H_0 terms and perturbation V terms. The H_0 terms are important in determining polaron band narrowing while the V terms are important in determining the correlation functions needed for calculating the diffusion coefficients, as briefly described below. Detail derivations and full formulation are non-trivial, and we wish to point the interested readers to [1] for more details.

Charge carrier mobility can be calculated based on the diffusion coefficient through the Einstein relationship as $\mu = e\beta D$, where e is the charge of the electron, $\beta = 1/k_B T$. In our theory, the diffusion coefficient can be obtained with:

$$D = a^2 \langle\langle v_k^2/(\Gamma_{kk} + \Gamma_0) + \gamma_{kk}\rangle\rangle \quad \text{(S4)}$$

where *a* is the nearest neighbor distance along the transport channel, *k* is the wave vector and $v_k = \nabla_k E_k$ is the polaron band velocity, Γ_0 is the scattering rate due to static disorder. The double bracket denotes the thermal average of the polaron state E_k, and Γ_{kk} and γ_{kk} are the scattering and hopping rates which can be further written as:

$$\Gamma_{kk} = N^{-1} \sum_{k \neq k'} W_{k,k;k',k'} \tag{S5}$$

$$\gamma_{kk} = \frac{1}{2} \nabla_q^2 \, Re \left(\frac{1}{2} W_{k,k;k'+q,k'+q} - W_{k,k+q;k',k'+q} \right) | q = 0 \tag{S6}$$

here $W_{k,k+q;k',k'+q}$ is a quantity crucial to the calculation of diffusion coefficient, which is related to the Fourier transform of the time-correlation function of $V_{k,k'}(t)$ as:

$$\begin{aligned} W_{k,k+q;k',k'+q} = \int_0^\infty dt \Big\{ \Big\langle V_{k'+q,k+q} V_{k,k'}(t) \Big\rangle \exp\Big[-i \left(E_{k'+q} - E_{k+q} \right) t \Big] \\ + \Big\langle V_{k'+q,k+q}(t) V_{k,k'} \Big\rangle \exp\Big[-i \left(E_k - E_{k'} \right) t \Big] \Big\} \end{aligned} \tag{S7}$$

The single bracket indicates the average of the residual interaction. Here the single angular bracket denotes the average of the residual interaction $V_{k,k'}(t)$ over phonon states. This residual interaction originates from the temperature-dependent canonical transformation. The major model parameters have been listed in Table 1 of the main text. Other model parameters involved are: a finite phonon bandwidth of $\Delta\omega = 0.1\ \omega_0$ (in which ω_0 is the characteristic phonon frequency, which describes the overall effect of all phonon modes and has the relationship of $E_{pol} = S\omega_0$) and a constant scattering rate Γ_0 (which can take the effects of impurities, static disorder, and low-frequency vibrational modes on band-like mobilities). ω_0 takes different values for electrons and holes considering the different nature of their transport channels, which are set as: ω_0 (electron)= 1426.0 cm^{-1} and ω_0 (hole)= 1525.5 cm^{-1}. The value of Γ_0 for electron transport has been set to 0.3 ω_0 by treating the low frequency (< 500 cm^{-1}) vibrational modes in DTTCNQ as a source of scattering while Γ_0 value has been set to 0.01 ω_0 for hole transport by solely considering the static disorder.

1.5 Calculation of hole and electron transport anisotropy.

The calculation of hole transport anisotropy follows a widely applied method.[7, 8] Based on the measured angles of θ_1 and θ_2, as well as calculated maximum hole mobility for transport channels along each dimer direction, we can calculate overall mobilities for different systems as:

$$\mu_{\text{electron}} = 0.030\cos^2\Phi + 1.095\cos^2(74.25-\Phi) + 1.095\cos^2(63+\Phi)\,, \quad \text{(S8)}$$

$$\mu_{\text{hole}} = 0.059\cos^2\Phi + 0.000\cos^2(47.5-\Phi) + 0.32\cos^2(65.9+\Phi)\,, \quad \text{(S9)}$$

The units for hole mobility are $cm^2\ V^{-1}\ s^{-1}$. In Table 1, we can see some dimer pairs may have higher transfer integral due to a different relative orientation between two molecules. Thus, we take the lower one to calculate for the maximum mobility along that dimer direction since these pairs are considered as the rate-limiting ones for the diffusion of hole-polarons.

1.6 Details of DFT calculations, charge decomposition analysis, and symmetry-adapted perturbation theory (SAPT) calculations.

We used CP2K[7] to relax the XRD-determined unit cells of the anthracene-DTTCNQ, anthracene, and DTTCNQ crystals with lattice parameters fixed experiment values. The convergence criteria have been set to that when both total force and RMSD force are lower than 1×10^{-4} $Bohr^{-1}Ha$. Also, maximum displacement and RMSD displacement should reach that lower than 1×10^{-3} Bohr. The self-consistent (SCF) convergence criterion has been set to that < 1×10^{-7} Ha. An energy cut-off of 300 Ha has been adopted. As for the pseudopotential, we have chosen the GTH potential[9-11] from Perdew-Burke-Ernzerhof (PBE) density functional. The Grimme's dispersion correction (G06)[12, 13] has been imposed in all DFT calculations. Both electron and hole transfer integrals were calculated via the VOTCA package[14] by adopting the method in [15]. Dimers were extracted according to the definition of transport channels, as shown in **Fig. S9-S10**. Molecular orbital needed were obtained from SCF calculations at the level of PW91/def2-TZVP with consideration of those suggested in [8] by using the Gaussian 09 (G09) [16] package. The other important transport parameter is the Huang-Rhys' factor *S* for electrons and holes. Here we applied the DUSHIN code[17] in conjunction with Gaussian 09 (G09)[16] calculations at the PBE0/def2-SVP[18] level to calculate S values. Both geometries of DTTCNQ/anthracene molecules with and without negative/positive charge were optimized free of symmetry constraints using closed-shell and open-shell (with spin multiplicity set to S=1/2) methods, respectively. Optimized geometries were then used for frequency calculations at the same level. We can calculate for the normal mode displacement Δ_k for the k_{th} vibrational mode with frequency ω_k of the charged state concerning the neutral state geometry based on the geometries of the DTTCNQ/anthracene at their charged and charge-neutral states, as well as their respective vibrational frequencies, ω_k. Thus, we can calculate the Huang-Rhys factor as $S_k = \Delta_k^2/2$. Based on both Huang-Rhys factor S of the k_{th} vibrational mode and respective frequencies, we can easily get the value of polaron binding energy E_{pol} with $E_{pol} = \sum_k S_k\omega_k$. With the calculated values of transfer integral and Huang-Rhys factor, we are able to calculate for the electron/hole mobilities of anthracene-DTTCNQ co-crystal at room-temperature using the 1D polaron transport model via the Einstein relationship of $\mu=e\beta D$, with more details of the model described by the section above. We also plotted the LUMO and HOMO orbital isosurfaces obtained from single point energy calculation at the B3PW91/cc-pVDZ level based on geometry optimized at PBE0/def2-SVP level or extracted from an optimized unit cell in **Fig. S5** to facilitate further discussions in the main text. Besides, S_k for all vibrational modes of anthracene and DTTCNQ and polaron binding energies are plotted in **Fig. S6-S8,** with scaled vector plots for the relatively strongly coupled modes (S≥ 0.05) provided to understand the role of molecular geometry in affecting electron/hole-vibrational coupling in DTTCNQ/anthracene molecules.

The charge decomposition analysis (CDA) is performed using the MultiWFN package version 3.6[19, 20] at the level of B3PW91/cc-pVDZ for the DFT-optimized anthracene-DTTCNQ stacking dimers. Further confirmation of the co-crystal nature of anthracene-DTTCNQ crystal at a higher theory level has been achieved via the SATP0 calculation. The used Psi4[21, 22] package version 1.1 is used to perform the SATP0 and SATP0-CT[23] calculation with a jun-cc-pVDZ basis set. We also performed SAPT0 calculation for the non-covalent interactions for the stacking dimers extracted from DFT-optimized anthracene and DTTCNQ unit cells.

1.7 Fig. S4. LUMO and LUMO+1 (upper panel) as well as HOMO and HOMO-1 (lower panel) isosurfaces for the acceptor-donor-acceptor (A-D-A) and donor-acceptor-donor (D-A-D) triads.

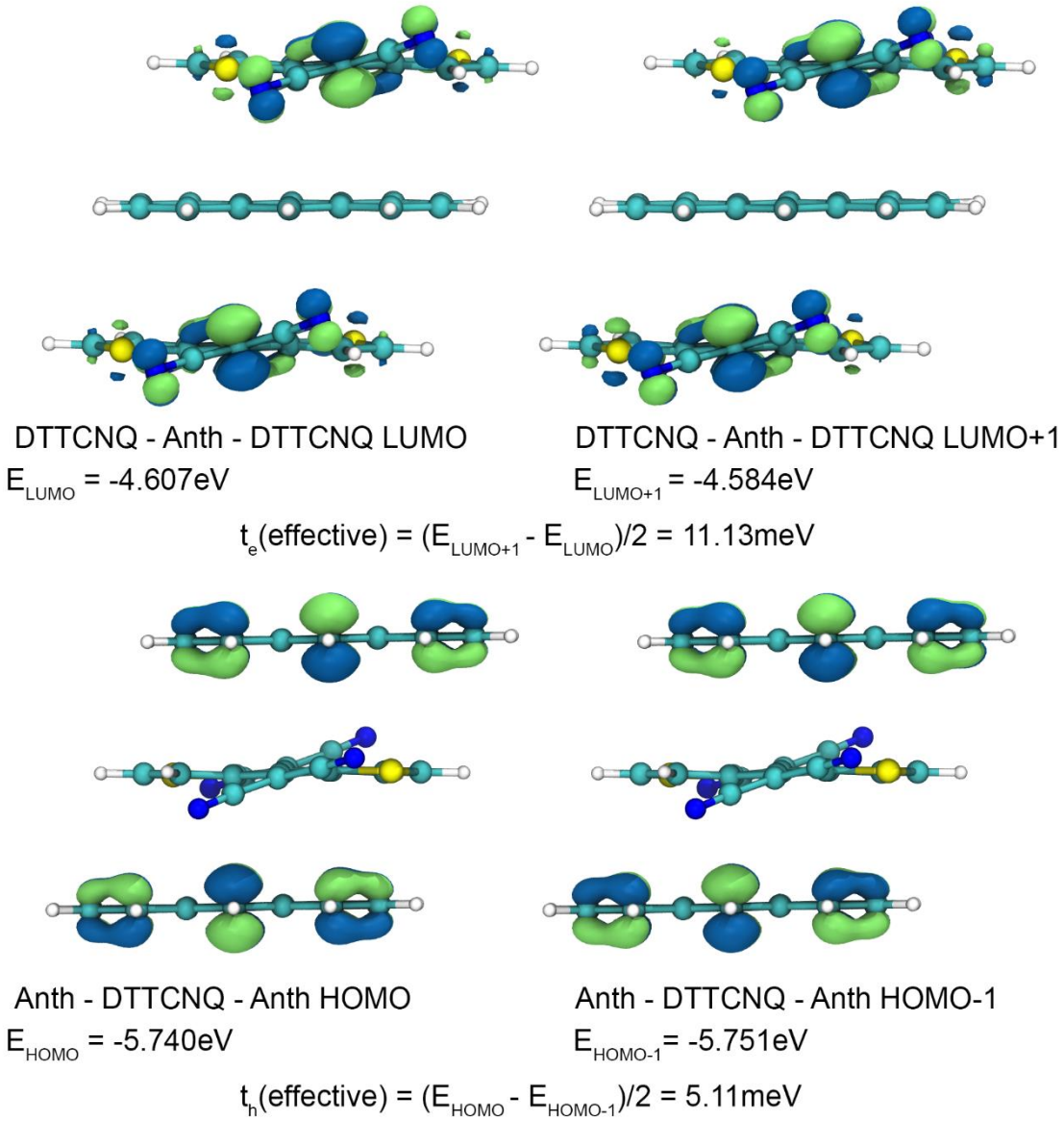

Fig. S4. LUMO and LUMO+1 (upper panel) as well as HOMO and HOMO-1 (lower panel) isosurfaces for the acceptor-donor-acceptor (A-D-A) and donor-acceptor-donor (D-A-D) triads and calculated values of effective electron and hole transfer integrals.[24] The isovalue of the isosurfaces is set to ±0.04 a.u., where lime and blue colors represent positive and negative values, respectively. Carbon, hydrogen, and nitrogen atoms are colored in cyan, white, and blue, respectively. The energy level corresponding to the gold electrode is plotted as a dashed line in the figure.

1.8 Fig. S5. HOMO and LUMO orbital isosurfaces of anthracene molecule, stacking dimer of anthracene-DTTCNQ co-crystal, and DTTCNQ molecule with DFT-optimized geometries.

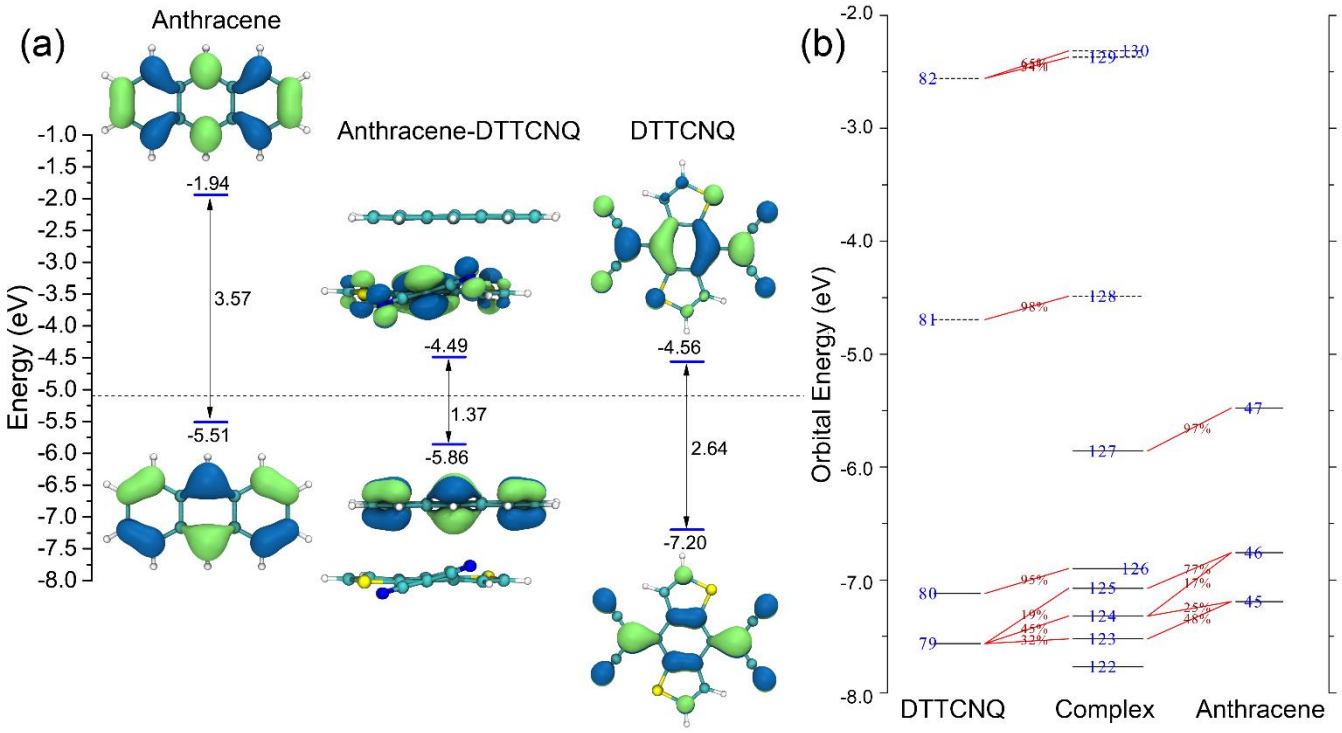

Fig. S5. (a) LUMO (upper panel) and HOMO (lower panel) orbital isosurfaces of anthracene molecule, stacking dimer of the Anthracene-DTTCNQ co-crystal and DTTCNQ molecule with DFT-optimized geometries. Respective orbital energies (with energy levels plotted) are also displayed with units of eV. The isovalue of the isosurfaces is set to ±0.04 a.u., where lime and blue colors represent positive and negative values, respectively. Carbon, hydrogen, and nitrogen atoms are colored in cyan, white and blue, respectively. The energy level corresponding to the gold electrode is plotted in a dashed line in **Fig.** S5b. The orbital interaction diagram is calculated from the CDA analysis. The virtual energy levels are shown as dash lines. Contributions of orbital from individual fragments to the complex are highlighted in red.

1.9 Fig. S6. Huang-Rhys factors for coupling between holes and different vibrational modes in anthracene with scaled vector plots.

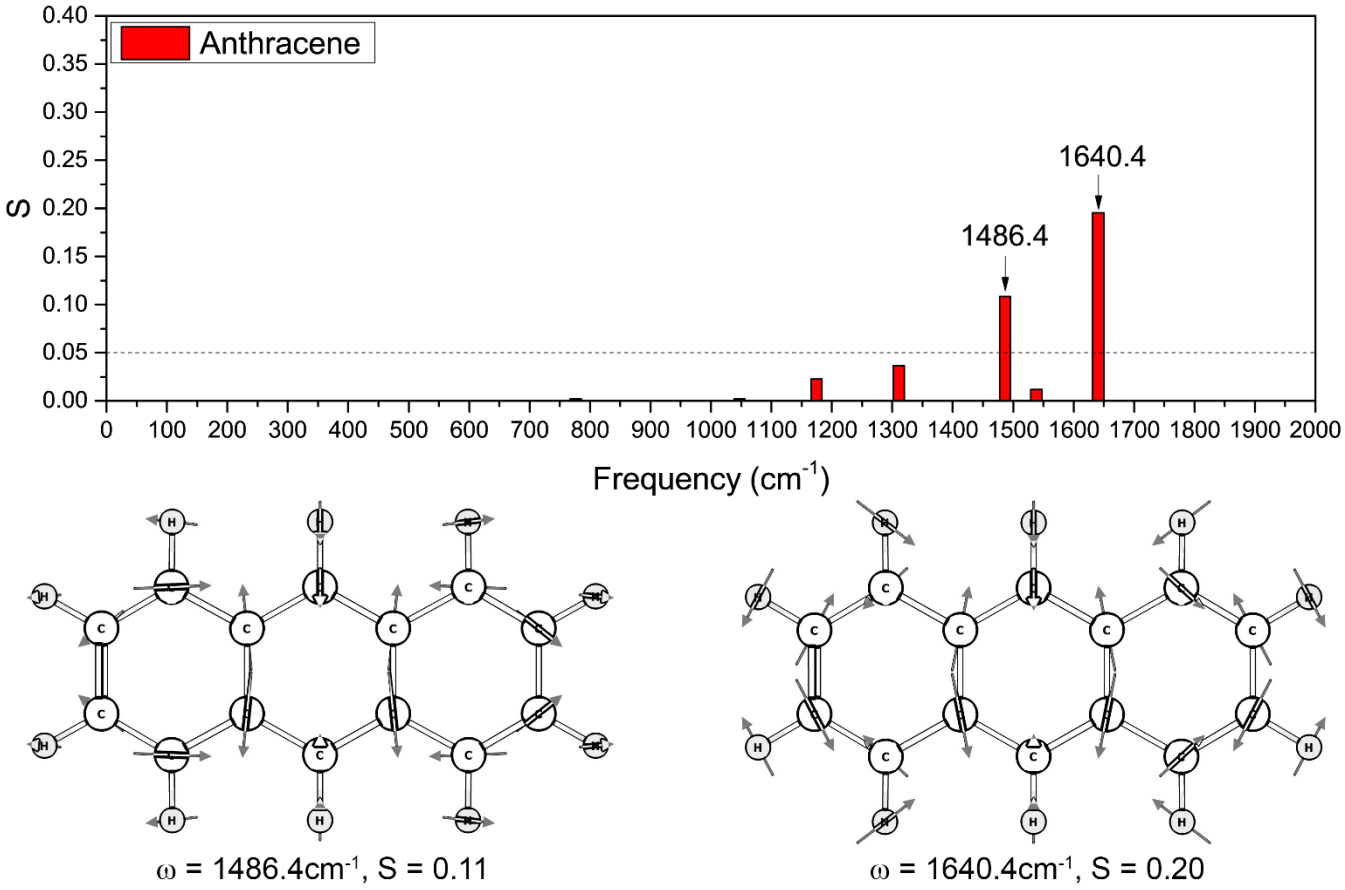

Fig. S6. Huang-Rhys factors for coupling between holes and different vibrational modes in anthracene with scaled vector plots of relatively strong coupling modes (S≥ 0.05) provided below the bar plots. The vector plots for the strong coupling vibrational modes are plotted using the ChemCraft package.

1.10 Fig. S7. Huang-Rhys factors for coupling between electrons and different vibrational modes in DTTCNQ with scaled vector plots.

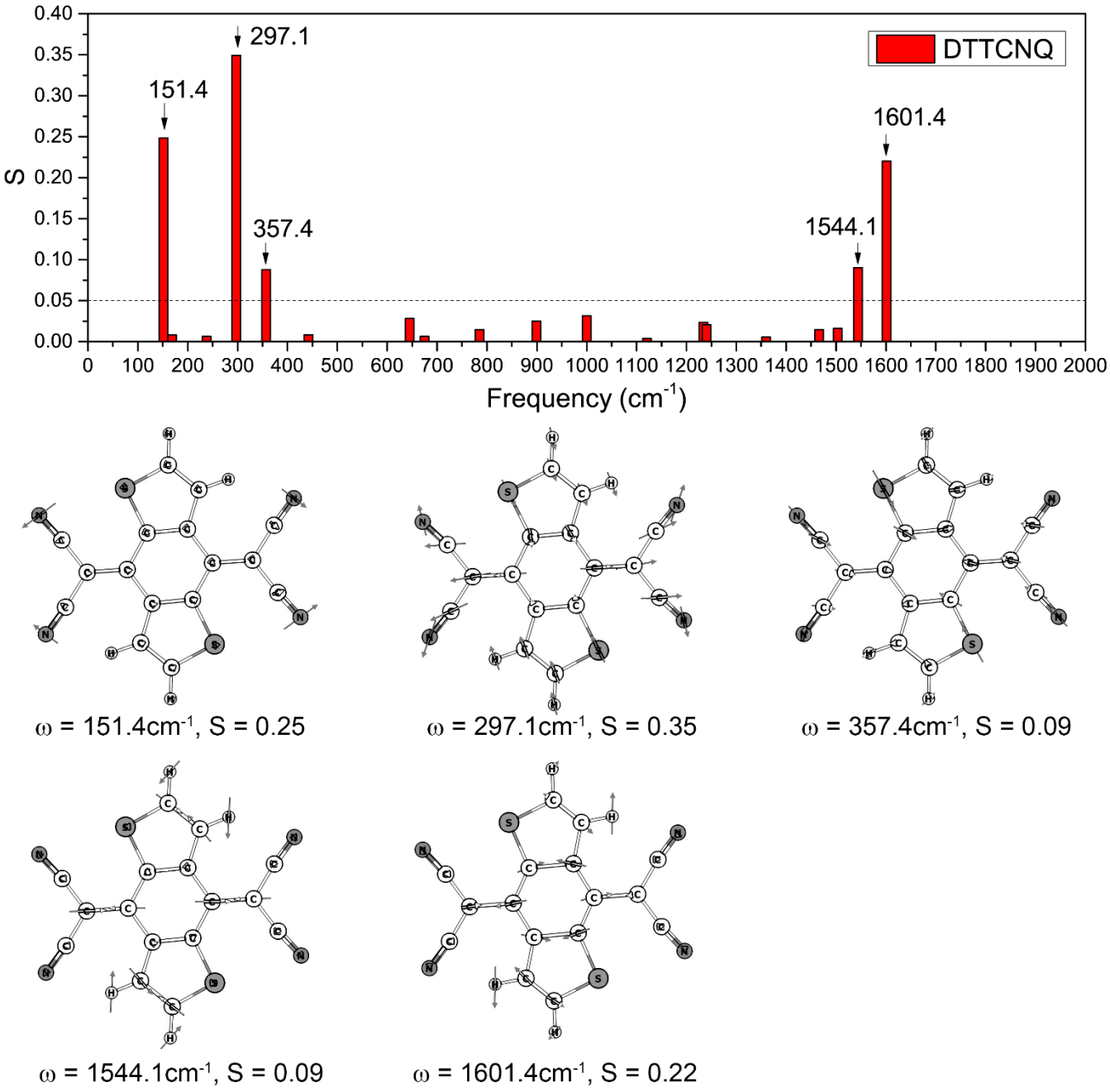

Fig. S7. Huang-Rhys factors for coupling between electrons and different vibrational modes in DTTCNQ with scaled vector plots of relatively strong coupling modes (S≥ 0.05) provided below the bar plots. The vector plots for the strong coupling vibrational modes are plotted using the ChemCraft package.

1.11 Fig. S8. Vibrational frequency-dependent polaron binding energies for holes in anthracene and electrons in DTTCNQ.

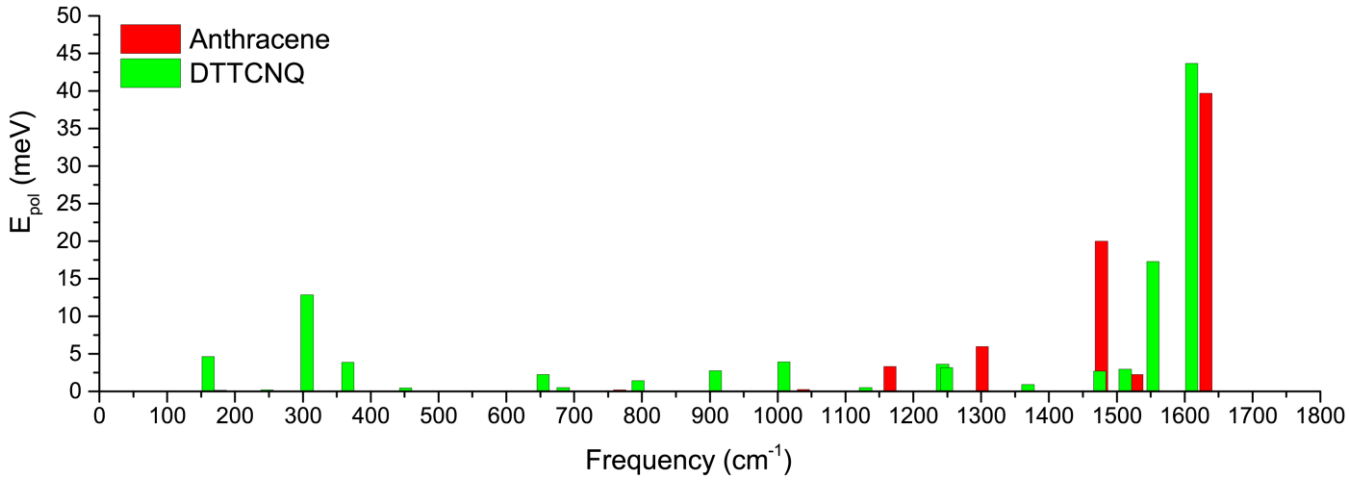

Fig. S8. Vibrational frequency-dependent polaron binding energies for holes in anthracene and electrons in DTTCNQ.

1.12 Fig. S9. Schematics of the separate-channel charge transport for the electron channels illustrated by the structure of two layers of anthracene-DTTCNQ co-crystal in the (011) surface with emphasis on DTTCNQ molecules and the dimer schematics in one layer of anthracene-DTTCNQ co-crystal with electron transport channel defined.

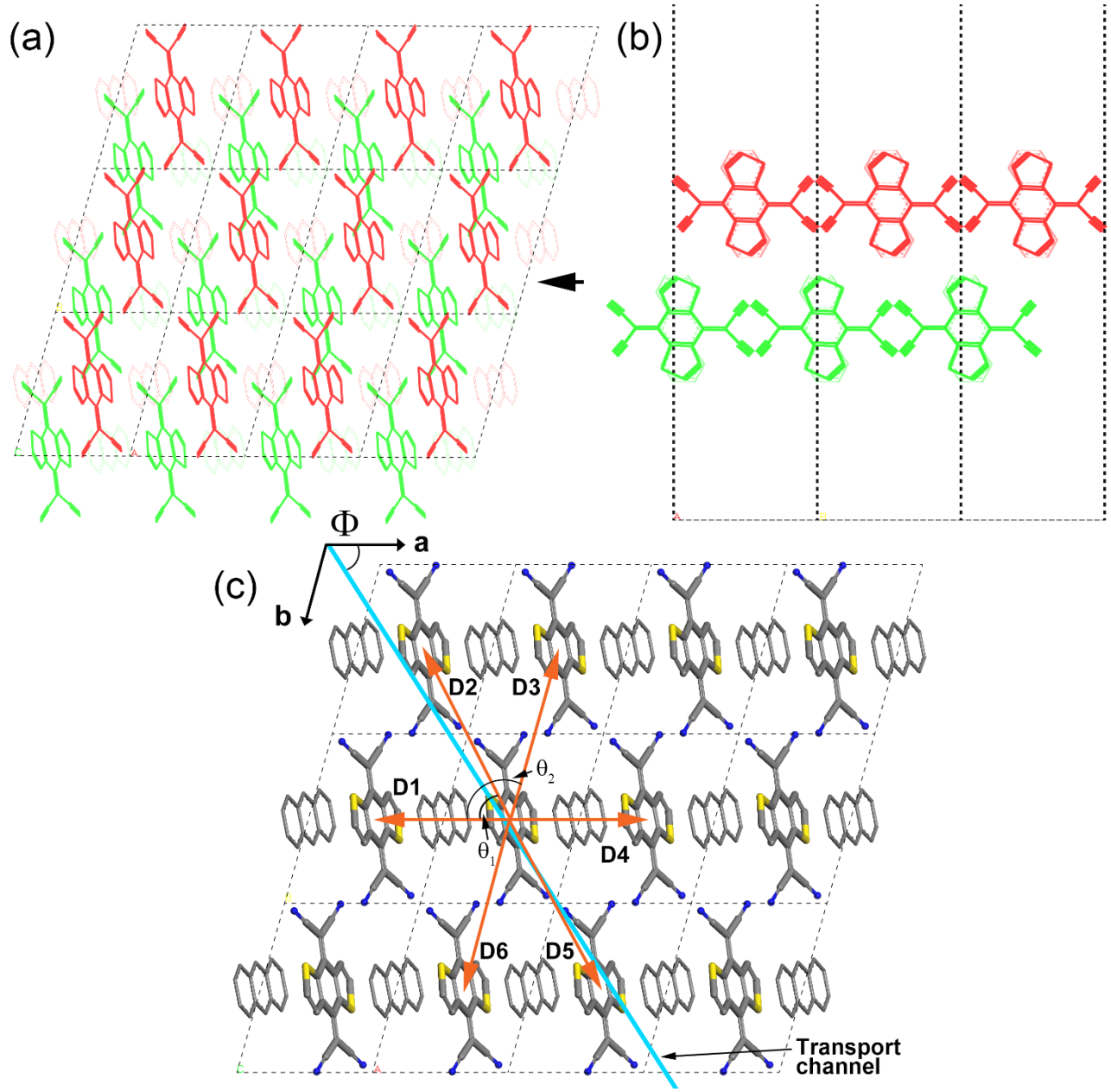

Fig. S9. Structure of (a) top view and (b) side view of two layers of anthracene-DTTCNQ co-crystal in the (011) surface with emphasis on DTTCNQ molecules. The viewing direction for (b) is pointed by the bold arrow in (a). The dimer schematics in one layer of anthracene-DTTCNQ co-crystal in the (011) surface is shown in (c), with the definition of dimers and transport channel for **electrons** also provided in the figure.

1.13 Fig. S10. Schematics of the separate-channel charge transport for the hole channels illustrated by the structure of two layers of anthracene-DTTCNQ co-crystal in the (011) surface with emphasis on anthracene molecules and the dimer schematics in one layer of anthracene-DTTCNQ co-crystal with hole transport channel defined.

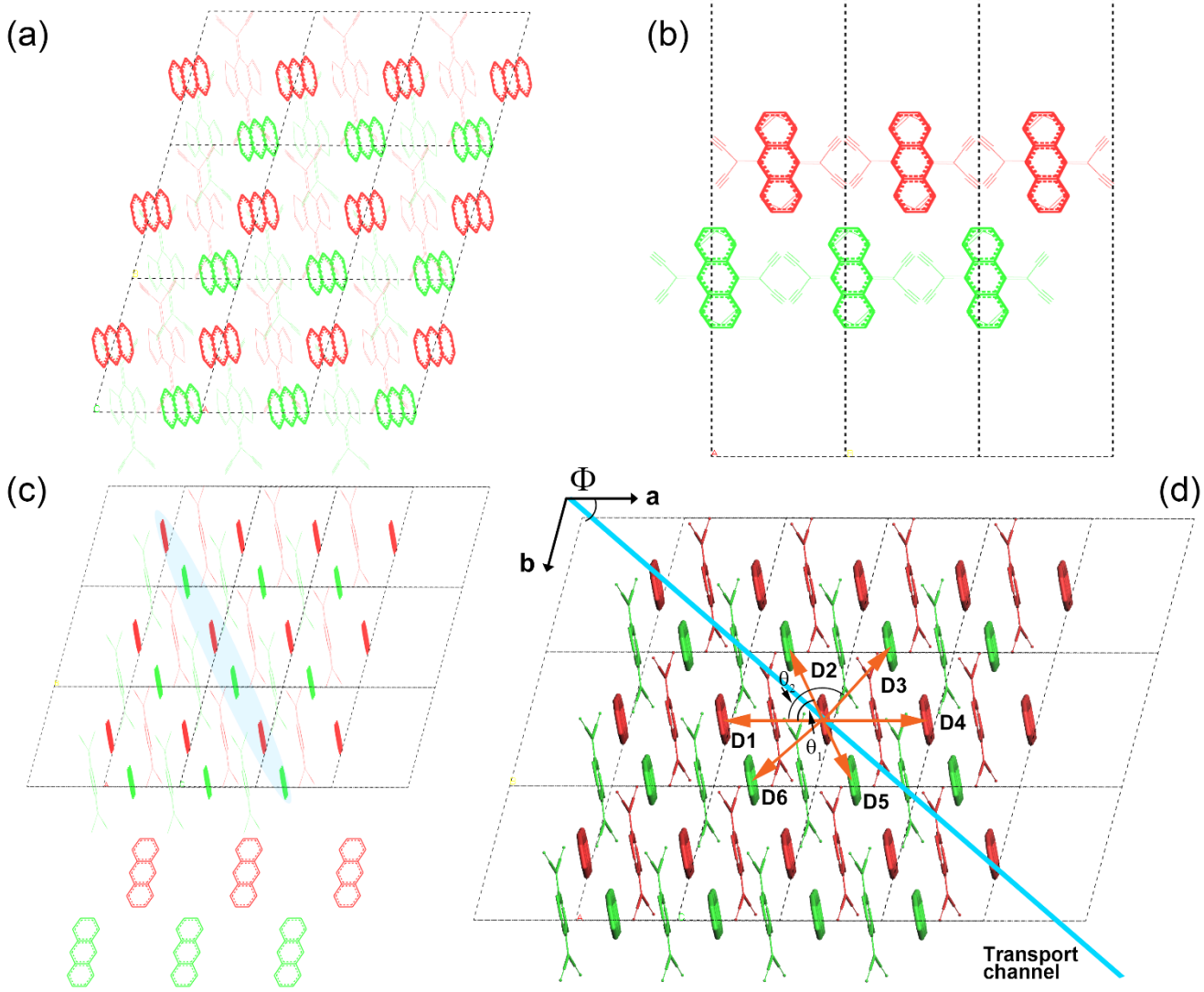

Fig. S10. Structure of (a) Top view and (b) side view of two layers of anthracene-DTTCNQ co-crystal in the (011) surface with emphasis on anthracene molecules. A slighted tilted top view of the (011) surface around the y-axis is plotted in (c), with extracted anthracene molecules highlighted in blue provided below. The dimer schematics in one layer of anthracene-DTTCNQ co-crystal in the (011) surface is shown in (d), with the definition of dimers and transport channel for **holes** also provided in the figure.

1.14 Table S1. Crystallographic data for anthracene-DTTCNQ co-crystal derived from single-crystal X-ray diffraction measurements.

	Anthracene-DTTCNQ
Formula	$C_{30}H_{14}N_4S_2$
Formula weight	494.57
Crystal system	triclinic
Space group	P -1
Lattice parameter a (Å)	7.3775(4)
Lattice parameter b (Å)	9.3783(6)
Lattice parameter c (Å)	9.4318(6)
Lattice parameter α (degree)	61.214(2)
Lattice parameter β (degree)	89.717(2)
Lattice parameter γ (degree)	73.611 (2)
Cell volume (Å3)	542.00(6)
Formula units per cell Z	1
Temperature (K)	100.(2)
m/mm^{-1}	0.71073 (Mo Kα)
F(000)	254
Reflections collected	3315
Independent reflections	3315
R1 (I > 2σ(I))	0.0686
wR(F2) (I > 2σ(I))	0.1285
R1 (all data)	0.1006
wR(F2) (all data)	0.1401
GOF	1.135

CCDC 1915403 (Anthracene-DTTCNQ) contains the supplementary crystallographic data for this paper. These data are provided free of charge by The Cambridge Crystallographic Data Centre (CCDC).

1.15 Table S2. The charge decomposition analysis (CDA) results obtained at B3PW91/cc-pVDZ Level. Here d, b, and r denote the number of electrons donated from fragment 1 to fragment 2, the number of electrons back donated from fragment 2 to fragment 1, and the number of electrons involved in repulsive polarization. Fragment 1 is DTTCNQ, and fragment 2 is anthracene in the stacking dimer of anthracene-DTTCNQ.

Orb.	Occ.	d	b	d-b	r	Orb.	Occ.	d	b	d-b	r	Orb.	Occ.	d	b	d-b	r
1	2	0.0000	0.0000	0.0000	0.0000	48	2	-0.0004	0.0000	-0.0004	0.0008	95	2	0.0001	0.0000	0.0001	0.0010
2	2	0.0000	0.0000	0.0000	0.0000	49	2	0.0000	0.0000	0.0000	0.0001	96	2	0.0006	0.0002	0.0004	0.0148
3	2	0.0000	0.0000	0.0000	0.0000	50	2	-0.0003	0.0000	-0.0003	0.0006	97	2	0.0001	0.0001	0.0000	-0.0019
4	2	0.0000	0.0000	0.0000	0.0000	51	2	0.0000	-0.0006	0.0006	-0.0013	98	2	-0.0006	0.0010	-0.0016	-0.1117
5	2	0.0000	0.0000	0.0000	0.0000	52	2	-0.0005	0.0000	-0.0005	0.0003	99	2	0.0002	0.0000	0.0002	-0.0001
6	2	0.0000	0.0000	0.0000	0.0000	53	2	-0.0005	0.0000	-0.0005	0.0029	100	2	0.0000	0.0002	-0.0002	0.0007
7	2	0.0000	0.0000	0.0000	0.0000	54	2	0.0000	-0.0005	0.0005	-0.0029	101	2	0.0006	0.0001	0.0005	-0.0029
8	2	0.0000	0.0000	0.0000	0.0000	55	2	-0.0001	-0.0003	0.0002	0.0038	102	2	0.0003	0.0000	0.0003	0.0001
9	2	0.0000	0.0000	0.0000	0.0000	56	2	-0.0002	-0.0001	-0.0001	-0.0030	103	2	0.0004	0.0000	0.0004	0.0008
10	2	0.0000	0.0000	0.0000	0.0000	57	2	0.0000	-0.0004	0.0004	0.0014	104	2	0.0001	0.0001	-0.0001	-0.0007
11	2	0.0000	0.0000	0.0000	0.0000	58	2	-0.0002	0.0000	-0.0002	-0.0008	105	2	0.0002	0.0000	0.0003	0.0001
12	2	0.0000	0.0000	0.0000	0.0000	59	2	-0.0004	0.0000	-0.0004	0.0008	106	2	0.0001	0.0000	0.0001	0.0005
13	2	0.0000	0.0000	0.0000	0.0000	60	2	0.0000	-0.0003	0.0003	-0.0010	107	2	0.0001	0.0017	-0.0016	-0.0197
14	2	0.0000	0.0000	0.0000	0.0000	61	2	-0.0004	0.0000	-0.0004	0.0001	108	2	0.0014	0.0000	0.0014	-0.0024
15	2	0.0000	0.0000	0.0000	0.0000	62	2	0.0000	-0.0003	0.0003	0.0001	109	2	0.0015	0.0000	0.0015	0.0018
16	2	0.0000	0.0000	0.0000	0.0000	63	2	-0.0001	0.0000	-0.0001	0.0002	110	2	0.0000	0.0000	0.0000	0.0010
17	2	0.0000	0.0000	0.0000	0.0000	64	2	0.0000	0.0000	0.0000	-0.0003	111	2	0.0001	0.0001	0.0000	0.0001
18	2	0.0000	0.0000	0.0000	0.0000	65	2	-0.0001	0.0000	-0.0001	0.0001	112	2	0.0003	0.0001	0.0002	-0.0005
19	2	0.0000	0.0000	0.0000	0.0000	66	2	0.0000	-0.0001	0.0001	0.0001	113	2	0.0003	0.0002	0.0002	-0.0021
20	2	0.0000	0.0000	0.0000	0.0000	67	2	-0.0002	0.0000	-0.0002	0.0001	114	2	0.0007	0.0002	0.0006	0.0065
21	2	0.0000	0.0000	0.0000	0.0000	68	2	-0.0002	0.0000	-0.0002	0.0011	115	2	0.0001	0.0001	0.0001	-0.0021
22	2	0.0000	0.0000	0.0000	0.0000	69	2	-0.0001	-0.0001	0.0000	-0.0004	116	2	0.0000	0.0001	-0.0001	-0.0023
23	2	0.0000	0.0000	0.0000	0.0000	70	2	-0.0002	0.0000	-0.0002	0.0007	117	2	0.0003	0.0000	0.0002	0.0013
24	2	0.0000	0.0000	0.0000	0.0000	71	2	0.0000	0.0001	-0.0001	-0.0002	118	2	0.0002	0.0003	-0.0002	-0.0075
25	2	0.0000	0.0000	0.0000	0.0000	72	2	0.0000	0.0000	0.0000	0.0000	119	2	0.0001	0.0028	-0.0027	-0.0145
26	2	0.0000	0.0000	0.0000	0.0000	73	2	0.0000	0.0000	0.0000	0.0003	120	2	0.0000	0.0025	-0.0024	-0.0242
27	2	0.0000	0.0000	0.0000	0.0000	74	2	0.0000	0.0000	0.0000	0.0002	121	2	0.0012	0.0007	0.0005	0.0139
28	2	0.0000	0.0000	0.0000	0.0000	75	2	0.0000	0.0000	0.0000	0.0001	122	2	0.0025	0.0004	0.0022	-0.0169
29	2	0.0000	0.0000	0.0000	0.0000	76	2	0.0000	0.0001	-0.0001	0.0002	123	2	0.0023	0.0022	0.0001	-0.0146
30	2	0.0000	0.0000	0.0000	0.0000	77	2	0.0000	0.0000	0.0000	0.0008	124	2	0.0013	0.0013	0.0000	-0.0371
31	2	0.0000	0.0000	0.0000	0.0000	78	2	0.0000	0.0000	0.0000	0.0003	125	2	0.0006	0.0041	-0.0035	-0.0580
32	2	0.0000	0.0000	0.0000	0.0000	79	2	0.0000	0.0001	-0.0001	-0.0001	126	2	0.0012	0.0002	0.0009	-0.0226
33	2	0.0000	0.0000	0.0000	0.0000	80	2	0.0000	0.0002	-0.0002	0.0003	127	2	0.0000	0.0089	-0.0089	-0.0195
34	2	0.0000	0.0000	0.0000	0.0000	81	2	-0.0001	0.0000	-0.0001	0.0006	128	0	0.0000	0.0000	0.0000	0.0000
35	2	0.0000	0.0000	0.0000	0.0000	82	2	-0.0002	0.0001	-0.0003	0.0368	129	0	0.0000	0.0000	0.0000	0.0000
36	2	0.0000	0.0000	0.0000	0.0000	83	2	0.0000	0.0001	-0.0001	0.0002	130	0	0.0000	0.0000	0.0000	0.0000
37	2	0.0000	0.0000	0.0000	0.0000	84	2	0.0000	0.0000	0.0000	0.0206	Sum:	254	0.0124	0.0267	-0.0143	-0.1657
38	2	0.0000	0.0000	0.0000	0.0000	85	2	0.0000	0.0000	0.0000	0.0001						
39	2	0.0000	0.0000	0.0000	0.0000	86	2	0.0000	0.0003	-0.0003	0.0083						
40	2	0.0000	0.0000	0.0000	0.0000	87	2	0.0000	0.0000	0.0000	0.0011						
41	2	0.0000	0.0000	0.0000	0.0000	88	2	0.0001	0.0000	0.0001	0.0009						
42	2	0.0000	0.0000	0.0000	0.0000	89	2	0.0006	0.0000	0.0006	0.0091						
43	2	0.0000	0.0000	0.0000	0.0000	90	2	0.0000	0.0001	-0.0001	-0.0041						
44	2	0.0000	0.0000	0.0000	0.0000	91	2	0.0000	0.0000	0.0000	0.0172						
45	2	-0.0007	0.0000	-0.0007	0.0012	92	2	0.0000	0.0002	-0.0002	0.0471						
46	2	-0.0002	0.0000	-0.0002	0.0002	93	2	0.0000	0.0002	-0.0002	0.0031						
47	2	-0.0002	0.0000	-0.0002	0.0003	94	2	0.0001	0.0001	0.0000	0.0050						

========== Extended Charge decomposition analysis (ECDA) ==========

Contribution to all occupied complex orbital:

Occupied, virtual orbitals of fragment 1: 7998.8359% 3.2215%

Occupied, virtual orbitals of fragment 2: 4696.8356% 1.1070%

Contribution to all virtual complex orbital:

Occupied, virtual orbitals of fragment 1: 1.1641% 25596.7785%

Occupied, virtual orbitals of fragment 2: 3.1644% 19898.8930%

PL(1) + CT(1→ 2) = 0.0233 PL(1) + CT (2→1) = 0.0644

PL(2) + CT(1→ 2) = 0.0221 PL(2) + CT (2→1) = 0.0633

The net electrons obtained by frag. 2 = CT (1→2) – CT (2→1) = -0.0411

PL stands for the polarization effect.

1.16 Table S3. The sSAPT0 and SATPT0-CT results for the stacking dimer in anthracene-DTTCNQ co-crystal, all values for sSAPT0 energies have units of kcal/mol. The schematics of the stacking dimers used for the SATP0 calculation can be found above the Table.

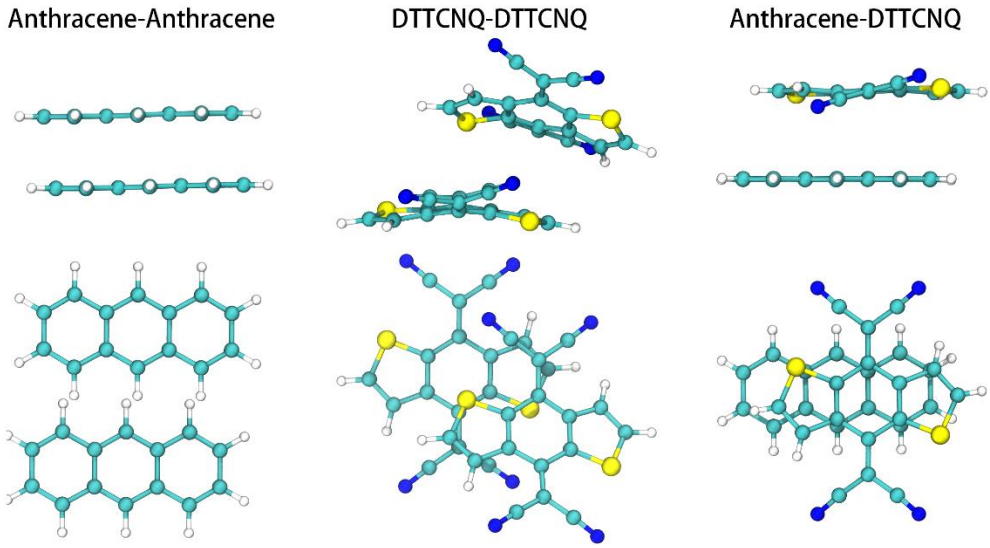

Item	Anthracene-DTTCNQ	Anthracene	DTTCNQ
Electrostatics sSAPT0	-10.967	-2.752	-5.553
Exchange sSAPT0	16.873	3.404	15.568
Induction sSAPT0	-2.173	-0.489	-2.733
Dispersion sSAPT0	-28.865	-6.045	-25.180
Total sSAPT0	-25.132	-5.882	-17.898
SAPT Induction (Dimer Basis)	-1.151		
SAPT Induction (Monomer Basis)	-0.992	N.A.	
SAPT Charge Transfer	-0.159		

2. References

1. D. Chen, J. Ye, H. Zhang and Y. Zhao, *J. Phys. Chem. B*, 2011, **115**, 5312-5321.
2. J. Ye, D. Chen and Y. Zhao, *J. Phys: Conf. Ser.*, 2012, **338**, 012018.
3. S. H. Wen, A. Li, J. L. Song, W. Q. Deng, K. L. Han and W. A. Goddard, *J. Phys. Chem. B*, 2009, **113**, 8813-8819.
4. R. W. Munn and R. Silbey, *J. Chem. Phys.*, 1985, **83**, 1854-1864.
5. R. W. Munn and R. Silbey, *J. Chem. Phys.*, 1985, **83**, 1843-1853.
6. R. Silbey and R. W. Munn, *J. Chem. Phys.*, 1980, **72**, 2763-2773.
7. J. Hutter, M. Iannuzzi, F. Schiffmann and J. VandeVondele, *WIREs Comput. Mol. Sci.*, 2014, **4**, 15-25.
8. W.-Q. Deng, L. Sun, J.-D. Huang, S. Chai, S.-H. Wen and K.-L. Han, *Nat. Protoc.*, 2015, **10**, 632-642.
9. S. Goedecker, M. Teter and J. Hutter, *Phys. Rev. B*, 1996, **54**, 1703-1710.
10. C. Hartwigsen, S. Goedecker and J. Hutter, *Phys. Rev. B*, 1998, **58**, 3641-3662.
11. M. Krack, *Theor. Chem. Acc.*, 2005, **114**, 145-152.
12. S. Grimme, *J. Comput. Chem.*, 2006, **27**, 1787-1799.
13. V. Barone, M. Casarin, D. Forrer, M. Pavone, M. Sambi and A. Vittadini, *J. Comput. Chem.*, 2009, **30**, 934-939.
14. V. Rühle, A. Lukyanov, F. May, M. Schrader, T. Vehoff, J. Kirkpatrick, B. Baumeier and D. Andrienko, *J. Chem. Theory Comput.*, 2011, **7**, 3335-3345.
15. E. F. Valeev, V. Coropceanu, D. A. da Silva Filho, S. Salman and J.-L. Brédas, *J. Am. Chem. Soc.*, 2006, **128**, 9882-9886.
16. M. J. Frisch, G. W. Trucks, H. B. Schlegel, G. E. Scuseria, M. A. Robb, J. R. Cheeseman, G. Scalmani, V. Barone, B. Mennucci, G. A. Petersson, H. Nakatsuji, M. Caricato, X. Li, H. P. Hratchian, A. F. Izmaylov, J. Bloino, G. Zheng, J. L. Sonnenberg, M. Hada, M. Ehara, K. Toyota, R. Fukuda, J. Hasegawa, M. Ishida, T. Nakajima, Y. Honda, O. Kitao, H. Nakai, T. Vreven, J. A. Montgomery Jr., J. E. Peralta, F. Ogliaro, M. J. Bearpark, J. Heyd, E. N. Brothers, K. N. Kudin, V. N. Staroverov, R. Kobayashi, J. Normand, K. Raghavachari, A. P. Rendell, J. C. Burant, S. S. Iyengar, J. Tomasi, M. Cossi, N. Rega, N. J. Millam, M. Klene, J. E. Knox, J. B. Cross, V. Bakken, C. Adamo, J. Jaramillo, R. Gomperts, R. E. Stratmann, O. Yazyev, A. J. Austin, R. Cammi, C. Pomelli, J. W. Ochterski, R. L. Martin, K. Morokuma, V. G. Zakrzewski, G. A. Voth, P. Salvador, J. J. Dannenberg, S. Dapprich, A. D. Daniels, Ö. Farkas, J. B. Foresman, J. V. Ortiz, J. Cioslowski and D. J. Fox, *Journal*, 2009.
17. J. R. Reimers, *J. Chem. Phys.*, 2001, **115**, 9103-9109.
18. C. Adamo and V. Barone, *J. Chem. Phys.*, 1999, **110**, 6158-6170.
19. T. Lu and F. Chen, *J. Comput. Chem.*, 2012, **33**, 580-592.
20. M. Xiao and T. Lu, *J. Adv. Phys. Chem*, 2015, **4**, 111-124.
21. J. M. Turney, A. C. Simmonett, R. M. Parrish, E. G. Hohenstein, F. A. Evangelista, J. T. Fermann, B. J. Mintz, L. A. Burns, J. J. Wilke, M. L. Abrams, N. J. Russ, M. L. Leininger, C. L. Janssen, E. T. Seidl, W. D. Allen, H. F. Schaefer, R. A. King, E. F. Valeev, C. D. Sherrill and T. D. Crawford, *WIREs Comput. Mol. Sci.*, 2012, **2**, 556-565.
22. R. M. Parrish, L. A. Burns, D. G. A. Smith, A. C. Simmonett, A. E. DePrince, E. G. Hohenstein, U. Bozkaya, A. Y. Sokolov, R. Di Remigio, R. M. Richard, J. F. Gonthier, A. M. James, H. R. McAlexander, A. Kumar, M. Saitow, X. Wang, B. P. Pritchard, P. Verma, H. F. Schaefer, K. Patkowski, R. A. King, E. F. Valeev, F. A. Evangelista, J. M. Turney, T. D. Crawford and C. D. Sherrill, *J. Chem. Theory Comput.*, 2017, **13**, 3185-3197.
23. A. J. Stone and A. J. Misquitta, *Chem. Phys. Lett.*, 2009, **473**, 201-205.
24. L. Zhu, Y. Yi, Y. Li, E.-G. Kim, V. Coropceanu and J.-L. Brédas, *J. Am. Chem. Soc.*, 2012, **134**, 2340-2347.